HAL
open science

Definition of a four-dimensional continuous planispheric transformation for the tracking and the analysis of left-ventricle motion

Jérôme Declerck, Jacques Feldmar, Nicholas Ayache

To cite this version:

Jérôme Declerck, Jacques Feldmar, Nicholas Ayache. Definition of a four-dimensional continuous planispheric transformation for the tracking and the analysis of left-ventricle motion. Medical Image Analysis, 1998, 2 (2), pp.197-213. 10.1016/S1361-8415(98)80011-X . inria-00615087

HAL Id: inria-00615087

https://inria.hal.science/inria-00615087v1

Submitted on 17 Aug 2011

HAL is a multi-disciplinary open access archive for the deposit and dissemination of scientific research documents, whether they are published or not. The documents may come from teaching and research institutions in France or abroad, or from public or private research centers.

L'archive ouverte pluridisciplinaire **HAL**, est destinée au dépôt et à la diffusion de documents scientifiques de niveau recherche, publiés ou non, émanant des établissements d'enseignement et de recherche français ou étrangers, des laboratoires publics ou privés.

Medical Image Analysis (1998) volume 4, number 1, pp 1–17
© Oxford University Press

Definition of a 4D continuous planispheric transformation for the tracking and the analysis of LV motion

Jérôme Declerck*, Jacques Feldmar and Nicholas Ayache

INRIA, Projet EPIDAURE
2004 route des Lucioles, B.P. 93
06 902 Sophia Antipolis Cedex, France

Abstract
Cardiologists assume that analysis of the motion of the heart (especially the left ventricle) can give some information about the health of the myocardium.
A 4D polar transformation is defined to describe the left ventricle (LV) motion and a method is presented to estimate it from sequences of 3D images. The transformation is defined in 3D-planispheric coordinates (3PC) by a small number of parameters involved in a set of simple linear equations. It is continuous and regular in time and space, periodicity in time can be imposed. The local motion can be easily decomposed into a few canonical motions (radial motion, rotation around the long-axis, elevation). To recover the motion from original data, the 4D polar transformation is calculated using an adaptation of the Iterative Closest Point algorithm.
We present the mathematical framework and a demonstration of its feasability on a series of gated SPECT sequences.

Keywords: motion tracking, heart, LV, motion analysis, 4D

Received ?; revised ?; accepted ?

INTRODUCTION

Cardiologists assume that the analysis of the motion of the heart (especially the left ventricle) can give some information about the health of the myocardium. A huge effort has been made in medical image processing to track and analyse the motion of the LV, but due to the complexity of the modeling, this topic remains an open research problem.

Modern techniques provide 3D images which describe either the anatomy of the heart (MRI, US, for instance) or its functionality (Nuclear Medicine SPECT or PET imaging, for instance). It is possible to get sequences of such images over the whole cardiac cycle; such sequences are real 3D movies of the motion of the heart. The cardiac motion, like the motion of any real object must be therefore described as a 4D continuous and regular transformation of time and space. With the modality we are using for our experiments (gated SPECT), the acquisition of an image lasts over several cardiac cycles; the gating procedure allows to reconstruct a 3D volume using information taken at similar times over different cardiac cycles, assuming that all the cycles are identical during the acquisition. In our protocol, we therefore suppose that the heart beats at a regular pace, this may not be the case for specific pathologies inducing irregularities of the cardiac pulse rate: these diseases are not supposed to be studied in this paper.

Many techniques have been proposed to track the LV motion. All of them attempt to find the correspondence between pairs of successive images. Most of the proposed methods in 3D define a model of the shape of LV surfaces (endocardium and/or epicardium), using classical snake-like models (McInerney and Terzopoulos, 1995; Shi *et al.*, 1994; Amini and Duncan, 1992), spring-mass meshes (Nastar, 1994) or more constrained generic surfaces such as free-deformed superquadrics (Bardinet *et al.*, 1996; Bardinet *et al.*, 1995) or volumetric superquadrics (Park *et al.*, 1996; Park *et al.*, 1994). The tracking is processed using conservation

*Corresponding author
(e-mail: jdecler@sophia.inria.fr)

constraints based on proximity constraints (Bardinet *et al.*, 1996; Bardinet *et al.*, 1995), differential properties of the surface (Clarysse *et al.*, 1995; Shi *et al.*, 1994; Amini and Duncan, 1992; Goldgof *et al.*, 1988) or is directly computed from displacement or velocity information obtained in some specific MR imaging techniques: tags (Radeva *et al.*, 1996; Kraitchman *et al.*, 1995; Young *et al.*, 1995; Denney and Prince, 1994; Park *et al.*, 1994) or phase contrast (Meyer *et al.*, 1995; Shi *et al.*, 1995). In other work, no shape model is computed: the tracking is processed directly from the volumetric image using optical flow methods (Gorce *et al.*, 1997; Song *et al.*, 1994), conservation of differential elements of isophotes (Benayoun *et al.*, 1995) or using similarities of the intensity levels (Thirion, 1995).

Unfortunately, because the correspondence is defined between two successive images, regularity and periodicity in time is not guaranteed. Only a few studies impose temporal continuity or periodicity in their model: these studies deal with segmentation of 2D (O'Donnell *et al.*, 1994) or 3D images (de Murcia, 1996; Matheny and Goldgof, 1995; Schudy and Ballard, 1979). Some other rare methods in 2D (Todd Constable *et al.*, 1994; McEachen *et al.*, 1994) or in 3D (Thirion, 1995; Nastar, 1994) perform a posteriori time filtering. Moreover, all these tracking techniques ((Park *et al.*, 1996; Park *et al.*, 1994) excepted) do not provide intuitive parameters describing characteristic motions without non-trivial computation (Bardinet *et al.*, 1996; Bardinet *et al.*, 1995; Young *et al.*, 1994). The 4D polar transformation (Declerck *et al.*, 1997) defined in this article aims to achieve four goals:

1. to define a class of transformation of **time** and **space** in which the **temporal continuity and periodicity** can be included,
2. to define a class of **highly constrained** transformations in order to have a **relevant** description of the LV motion with a **reduced** number of parameters,
3. to be able to retrieve canonical motions with minimal computation, providing an easy-to-interpret **quantitative analysis** of the motion.
4. last, but not least, to be a transformation which combines the unknown parameters **in a linear way** to make their estimation easier and robust.

We shall see that all these points are achieved in the mathematical formulation that we propose below.

The paper is organised as follows: in section 1, we define the 4D polar transformation and the way to estimate it from a 4D (3D + time) data set. In section 2, a method is proposed to track in 4D the motion of the LV. Experiments have been conducted with a synthetic heart model and a gated SPECT sequence are presented in section 3. Section 4 draws conclusions concerning this work, its potential uses and future perspectives.

1. DEFINITION OF THE 4D PLANISPHERIC TRANSFORMATION

The idea of this study is to define a continuous and regular transformation of time and space. This transformation should also be adapted to describe with a minimum of parameters a complex motion such as the LV motion. This model of the deformation of the LV is a crude approximation compared to complex biomechanical models (Hunter and Smaill, 1988) or highly descriptive kinematic models (Arts *et al.*, 1992).

Given a point P (x, y, z) in cartesian coordinates and a time value t, the transformation gives a point Q (x', y', z') which is assumed to be the location of point P at time t. The cardiac motion is supposed to be regular in space and periodic in time. We therefore look for a **differentiable** function in spatial variables x, y and z and for a **differentiable** and a potentially **periodic** function in time variable t.

$$\begin{array}{rcl} f : \mathbb{R}^3 \times \mathbb{R} & \longrightarrow & \mathbb{R}^3 \\ (P,t) & \longmapsto & Q = f(P,t) \end{array}$$

This definition of the 4D transformation yields the definition of 2 categories of functions which are easier to understand and which are intrinsically regular (figure 1):

$$\begin{array}{rcll} T_P & = & f(P,\cdot) & \text{is the trajectory of } P \text{ over time,} \\ D_t & = & f(\cdot,t) & \text{is the instantateneous deformation} \\ & & & \text{function of the object at time } t. \end{array}$$

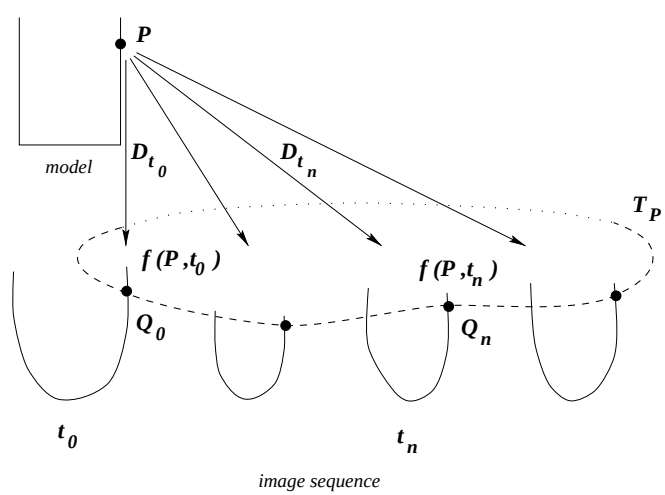

Figure 1. The model is deformed at every time of the image sequence. Point P at time t_n is point Q_n. Functions of instantaneous deformation D_{t_n} and the trajectory function T_P are illustrated.

In this paper, f is defined in order to describe locally some specific motions of points on the myocardium. We approximate the shape of the left ventricle as a stretched sphere in the long-axis direction. This is, of course, a very crude approximation as the shape of the heart is much more complex, however our goal is not a precise definition of the shape of the muscle, but a plausible discrimination of characteristic motions.

For that particular purpose, we separate the motion of a point of the heart into three canonical orthogonal motions (figure 2):

- motion 1: a **radial motion** which decribes the contraction or dilatation of the whole structure towards a "center" ;
- motion 2: a **apico-basal rotation** around the apico-basal axis which describes the twisting motion of the LV points ;
- motion 3: a motion (tangential to the surface $r = C^t$) which describes the **elevation** of the LV points in the apico-basal direction (the shortening along the long-axis during the systole).

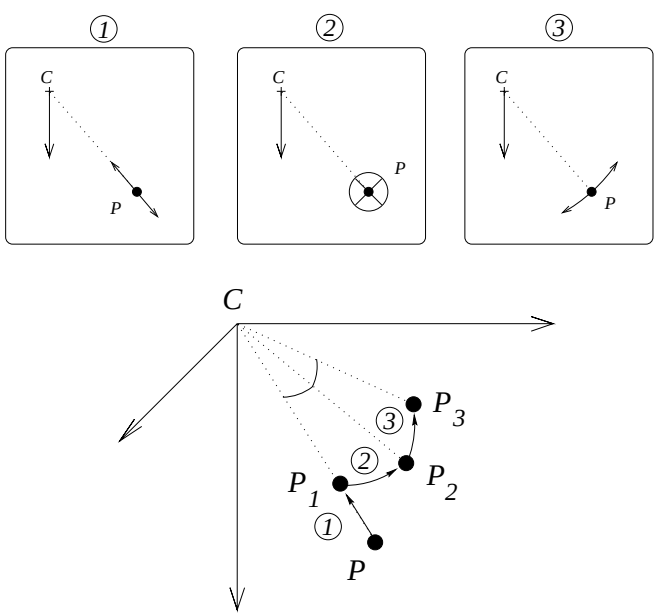

Figure 2. The top three frames illustrate the orthogonal motions described in the text. Bottom, point P is transformed in P_1 by the first motion (radial motion), P_1 is transformed in P_2 by the second (apico-basal rotation) and P_2 is transformed in P_3 by the third one (elevation).

We describe these motions in a "3D-planispheric" coordinates (3PC) system, which is a combination of spherical and cylindrical coordinates. Our tranformation function is thus defined as a composition of three functions:

$$f \quad = \quad P2C \circ F \circ C2P$$

The function $C2P$ switches from cartesian to 3PC, $P2C$ switches back from 3PC to cartesian coordinates (of course, $C2P = P2C^{-1}$). F is the function which is described with the three basic motions in 3PC. The next two paragraphs detail the definitions of these functions.

1.1. Cylindrical or planispheric coordinates ?

The approach is inspired from (Park *et al.*, 1996; Park *et al.*, 1994): in that study, the equations for the deformation of the superquadric model is expressed in cylindrical coordinates. In such coordinates, the decomposition of the local motion in our three canonical motions does not have the same relevance if the point where they are estimated belongs to a lateral wall (where the muscle is roughly cylindrical) or if the point is close to the apex (where the muscle is roughly spherical). For instance, a point belonging to a lateral wall and animated by an axial contraction does effectively contract towards the cylindrical axis (motion 1), but a point close to the apex animated with a similar motion does not contract, but undergoes a shift tangential to the wall. Thus, this motion is a twist (motion 2) or an elevation (motion 3) rather than a contraction (motion 1) (figure 3). We find it easier and more relevant to

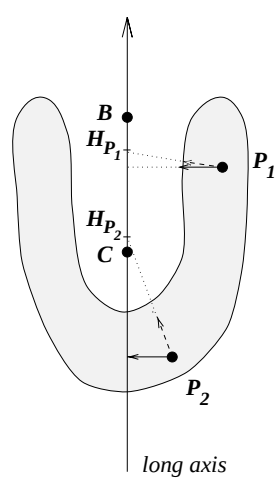

Figure 3. P_1 belongs to a lateral wall, P_2 is close to the apex, both points are animated with motion 1. Solid arrows describe the motion in cylindrical coordinates (contraction towards the apico-basal axis) and dotted arrows describe the motion in spherical coordinates (contraction towards the center C). Motion 1 effectively describes a contraction for P_1, but not for P_2.

use 3D-planispheric coordinates rather than cylindrical ones to decompose the local motion of points of the myocardium.

1.2. 3D-Planispheric coordinates

C2P : in 3D cartesian space, we define a 3D-planispheric reference system given a center C, a base B and a set of two orthogonal vectors u and v (figure 7). In order to fit with our description of the heart, we choose u as a vector parallel to the apico-basal direction, and v parallel to the septo-lateral direction. C is chosen in the center of the cavity, and B in the center of the base.

For each point P (x, y, z), a center point H_P is defined on line (CB). From this center point, a distance and two angles (latitude θ and longitude ϕ) are calculated just as in the classical spherical coordinate system. In the spherical system, H_P is the center C. In the cylindrical system, H_P is the orthogonal projection of P on the line CB. Our purpose here is to define a **combination of both spherical and cylindrical** coordinate systems (figure 4), in order to describe the position of P in "roughly" spherical coordinates around the apex (where the shape of the LV is roughly spherical) and in "roughly" cylindrical coordinates around the base (where the shape of the LV is roughly cylindrical). In our system, the position of H_P on the line CB is given by the simple formula:

$$CH_P = (1-\cos\theta)\, CB \qquad (1)$$

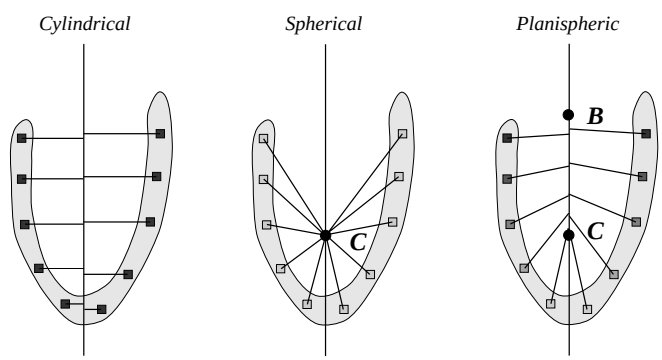

Figure 4. 3D-planispheric geometry is a combination of both cylindrical and spherical geometries.

- For low values of θ (P around the apex), H_P is close to C and shifts away from C with a distance increasing with $\frac{\theta^2}{2}$: around the apex, the 3PC system is thus close to the spherical one.
- For θ around $\frac{\pi}{2}$ (P around the apex), H_P is close to B, the distance BH_P varies linearly with $\theta - \frac{\pi}{2}$, and PH_P is nearly orthogonal to CB: around the base, the 3PC system is close to the cylindrical one (figure 7).

Of course, (1) is an implicit formula: H_P gives the angle θ, but we need θ to locate H_P. appendix A details the method we have developed to compute the location of H_P given a point P in space.

In our 3PC system, a surface of constant r is represented as a disk in a plane, like in a classical map projection in topography (this is why we use the word "planispheric"). The coordinates X, Y and R in this system are defined as follows:

$$\begin{aligned} X &= \frac{\theta}{\pi}\cos(\phi) \\ Y &= \frac{\theta}{\pi}\sin(\phi) \qquad (2) \\ R &= \frac{r}{\sigma_r} \end{aligned}$$

where σ_r is a normalization coefficient so that X, Y and R are dimensionless and vary within a similar range of values. Figure 5 illustrates the correspondence between the (x, y, z)

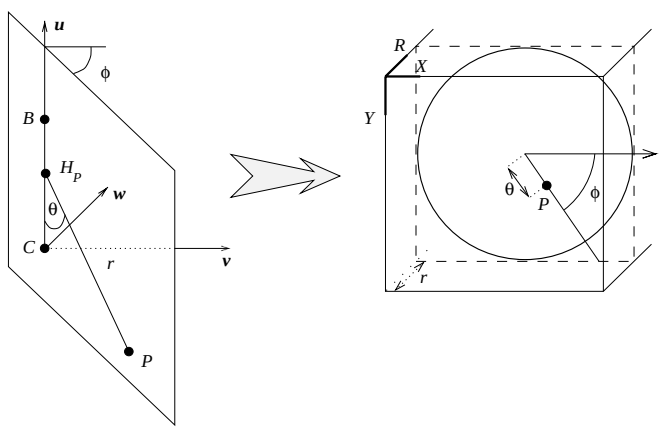

Figure 5. the cartesian coordinates (x,y,z) of point P are converted into polar coordinates in the 3D-planispheric image, the depth R is the distance from the point H_P in the cartesian image, the position (X,Y) in the plane is defined with the two angles θ and ϕ, like in the 2D-planispheric mapping.

cartesian coordinates and the (X, Y, R) coordinates in the 3PC system. In this system, apex point ($X = 0, Y = 0$) is the "south pole" of the projection, the points on the circle $X^2 + Y^2 = 1$ ($\theta = \pi$) are the same cartesian point, the "north pole" of the projection, featuring a point in the direction of the base or of the aorta. Around this point, the distorsion between the cartesian and our planispheric representation is maximum, but there should not be any cardiac points in this area (figure 6).

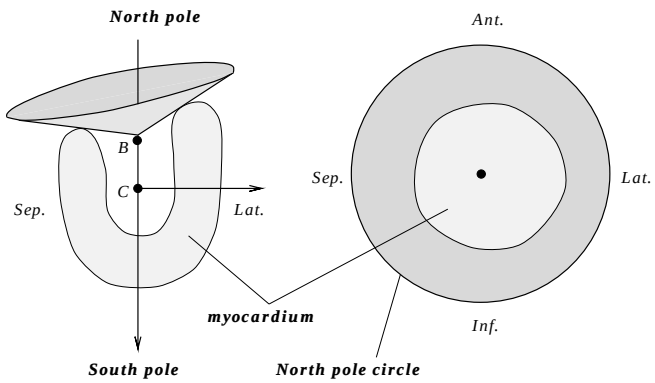

Figure 6. Left, the myocardium. From the center C, the limit of the basis draws a cone (dark gray) around the north pole. Right, in the 3D-planispheric map, the left ventricle (light gray) appears like a plate, the cone is a circular stripe around the heart.

P2C : conversely, given a point (X, Y, R) in the 3PC system so that $X^2+Y^2 \leq 1$, we can compute its cartesian coordinates (x, y, z) by calculating $\theta = \pi\sqrt{X^2+Y^2}$ and ϕ without ambiguity with the expressions of $cos(\phi)$ and $sin(\phi)$. The center H_P is calculated with (1).

The coordinate system we use is similar to the prolate spheroidal coordinates (PSC) system described in the litterature (Waks *et al.*, 1996). The equations are presented in appendix B, figure 7 shows ten surfaces of constant R in each of the two systems. There are three minor differences between the two systems:

1. the surfaces of constant R (for R values around what they should be to describe an average LV) are narrower around the apex than in the 3PC system: the shape of these surfaces is closer to the shape of an average LV;

2. there is an interval of R for which surfaces of constant R are close to a shape of an average LV. For those values, the location of point C is closer to the apex in the PSC system than in the 3PC, potentially yielding to forbidden intersection of segment $[CB]$ with the myocardial wall;

3. the surfaces of constant θ are cones in the 3PC system, they are confocal one-sheet hyperboloids in the PSC system. The local coordinates are orthogonal in PSC, whereas they are approximately orthogonal in 3PC. On the other hand, the decomposition of the motion is less intuitive in the PSC system.

In the sequel of this article, we concentrate on the 3PC system in order to obtain a closer approximation of the LV shape and a more intuitive decomposition of the motion.

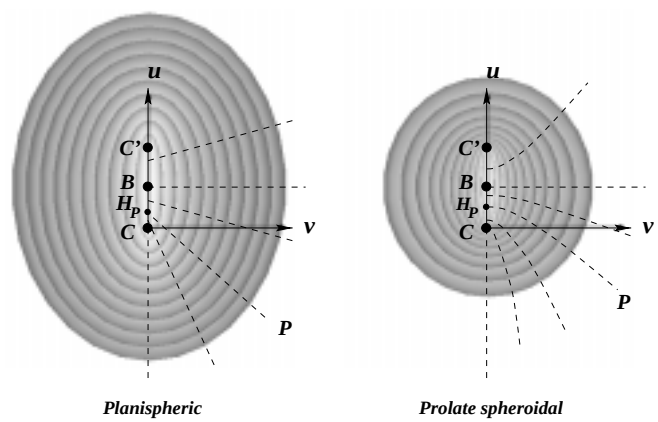

Figure 7. A representation of ten surfaces of constant R, on the left, in the 3PC system, on the right, in the prolate spheroidal. The dashed lines show different curves of constant θ: on one, a point P and its associated center H_P. Figure from (Declerck *et al*,1997).

1.3. The function in 3D-planispheric coordinates

In the 3D-planispheric system, given a point P (X, Y, R), the transformed point Q (X', Y', R') through F is expressed as follows:

$$\begin{aligned} X' &= a_0X - a_1Y + a_2 \\ Y' &= a_1X + a_0Y + a_3 \\ R' &= a_4R + a_5 \end{aligned} \tag{3}$$

X' and Y' are defined by a similarity function applied to X and Y. A similarity is a combinate of a 2D rotation by angle α, a uniform scaling of ratio k and a translation. R' is defined as an affine function of R. The similarity and the affine parameters a_p $(p = 0 \ldots 5)$ are continuous and differentiable functions of r, θ, ϕ and t.

Defining the transformation in the 3PC system allows to write: a) linear expressions in the parameters a_p, b) a simple computation of the canonical motion decomposition (radial motion, rotation, elevation) from the a_p and, c) a very compact description of the deformation.

1.3.1. Analysis of the motion in the canonical decomposition

Our canonical motions are retrieved with the following formulae:

1. the **radial motion** ratio (motion 1) is given by:

$$\frac{R'}{R} = a_4 + \frac{a_5}{R} \tag{4}$$

2. the linear relationships between X', Y' and X, Y define a 2D similarity such that

$$k = \sqrt{a_0^2 + a_1^2} \quad (5)$$

$$\alpha = \text{atan2}(\frac{a_1}{k}, \frac{a_0}{k}) \quad (6)$$

α is the **rotation** around the long-axis (motion 2) in 3PC;

3. k is the scale factor corresponding to an **elevation** magnification in latitude, which is our motion 3. In our display, we compute $\frac{\theta' - \theta}{\theta}$.

The 4D polar transformation is defined once the parameters a_p are determined. Because of the simplicity of (5) and (6), it is possible to easily analyse the motion using the parameters a_p. Because the variation of the parameters a_p is smooth and regular with variables r, θ, ϕ and t, the parameters which describe our canonical motions are also smooth and regular in time and space.

1.3.2. Degrees of freedom of the parameters, time dependency as a hard constraint

In order to define a smooth and continuous 4D transformation, the parameters depend on the location of the point and the instant at which the transformation is calculated. In our formulation, we choose the parameters as polynomial functions in r and θ and quadratic periodic B-splines (Risler, 1991; Farin, 1989) in ϕ and t:

$$a_p(r,\theta,\phi,t) = \sum_{i=0}^{n_r-1} \sum_{\substack{j=0 \\ j\neq 1}}^{n_\theta} \sum_{k=0}^{n_\phi-1} \sum_{n=0}^{n_t-1} A^p_{i,j,k,n} \left(\frac{r}{\sigma_r}\right)^i \left(\frac{\theta}{\pi}\right)^j B^\Phi_k(\phi)\, B^T_n(t) \quad (7)$$

for $p = 0\ldots4$. If we keep for a_5 an expression like (7), a_4 and a_5 are correlated because $R = \frac{r}{\sigma_r}$. We therefore simplify a_5 as follows:

$$a_5(r,\theta,\phi,t) = \sum_{\substack{j=0 \\ j\neq 1}}^{n_\theta} \sum_{k=0}^{n_\phi-1} \sum_{n=0}^{n_t-1} A^5_{j,k,n} \left(\frac{\theta}{\pi}\right)^j B^\Phi_k(\phi)\, B^T_n(t) \quad (8)$$

with the following notation:

- n_r is the number of parameters which define the polynomial function of variable r: the degree of this polynomial is $n_r - 1$.
- n_θ is the number of parameters which define the polynomial function of variable θ: to be differentiable in points for which $(\theta = 0)$, the polynomial must have no term in θ ($a_p(\theta) = a_p^0 + a_p^2\theta^2 + a_p^3\theta^3\ldots$). a_p is therefore a polynomial of θ of degree n_θ.
- n_ϕ is the number of control points of the B-spline periodic curve of variable ϕ. B^Φ are the B-spline basis functions associated to a classical regularly distributed 2π-periodic set of knots.
- n_t is the number of control points of the B-spline curve of variable t. B^T are the B-spline basis functions associated to a classical regularly distributed set of knots, this basis can be periodic or not.

The originality of the transformation is in the fact that the continuity and potentially the periodicity in time is a "hard" constraint. We can **implicitly look for time-periodic transformations**.

Using quadratic B-splines (with a set of regularly distributed knots in our current implementation) ensures C^1 continuity in ϕ and t; the function $a_p(r,\theta,\phi,\cdot)$ is a (potentially periodic) piecewise polynomial. Due to the definition of B-splines, the influence of possible outliers remain local (Risler, 1991).

To ensure the continuity for $\theta = 0$, we must impose the constraint $A^p_{i,0,k,n} = A^p_{i,0,0,n}$ for each k. There are thus $n_\phi - 1$ equations for each i and n. Finally, we get a number of control points $N_{CP} = (5.n_r + 1).(n_\phi.(n_\theta - 1) + 1).n_t$.

The transformation is completely defined given a center C and two orthogonal vectors (they define the 3PC system) and a set of N_{CP} control points (real numbers) $A^p_{i,j,k,n}$.

1.4. Estimation of a 4D planispheric transformation

1.4.1. The least squares criterion

Having a set of matches (P_l, $Q_{n,l}$) for different times t_n ($n = 0\ldots T-1$), we define a least squares criterion to estimate the 4D planispheric transform which could "best" fit the list of matches:

$$\forall n \in 0\ldots N-1, \qquad \forall m \in 0\ldots M-1, \qquad f(P_l, t_n) \simeq Q_{n,l} \quad (9)$$

The least squares criterion is therefore written:

$$J(f) = \sum_{n=0}^{T-1} \sum_{l=0}^{N-1} \alpha_{n,l}\,.\,d(\,f(P_l,t_n)\,;\,Q_{n,l}\,)^2 \quad (10)$$

where $d(\cdot;\cdot)$ is the distance and $\alpha_{n,l}$ is the weight related to the reliability of the match (P_l, $Q_{n,l}$).

If we choose the euclidean distance for d in cartesian coordinates, the criterion is not quadratic in the $A^p_{i,j,k,n}$, and its derivatives with respect to the $A^p_{i,j,k,n}$ are very difficult to linearize. We prefer to choose for d the euclidean distance expressed in 3PC ($X^2+Y^2+R^2$). The criterion is then quadratic in the $A^p_{i,j,k,n}$. d is a distance if and only if $X^2+Y^2<1$ (i.e. iff (X,Y) does not belong to the circle of the "north pole" of the planispheric map). As the center C is well inside the cavity and the base point B is in the center of the base circle, we are sure that all data points remain in a "security" cylinder in the 3PC system (maximum expected value for θ is around $\pi/2$, so X and Y are less than 0.5. See figure 6).

1.4.2. Minimization of the criterion

The criterion expressed with d as the euclidean distance in 3PC is quadratic in the control points $A^p_{i,j,k,n}$. Differentiating it with respect to $A^p_{i,j,k,n}$ gives a linear system which is solved with a classical conjugate gradient method. The size of the matrix is $(5.n_r+1).(n_\phi.(n_\theta-1)+1).n_t$. In fact, the linear system can be split in two independent subsystems, one for a_0, a_1, a_2, a_3 and the other for a_4 and a_5.

Assembling the matrix is an operation which obviously depends linearly with the N, the number of matches. Solving the linear system is an operation which depends on N_{CP}, the size of the matrix : a classical conjugate gradient needs $O({N_{CP}}^2)$ elementary operations per iteration. In our experiments, the $O(N)$ operation is much more costly than the $O({N_{CP}}^2)$ one (ratio is approximately 5:1).

2. TRACKING THE 4D MOTION OF THE LV

We define in this section an adaptation of the Iterative Closest Point algorithm (Besl and McKay, 1992; Zhang, 1994) which gives an estimation of those matches for the least squares minimization: it is possible this way to calculate the "best" function with respect to a distance criterion.

The motion is tracked in a heart image sequence (in our experiments, gated SPECT). Points featuring the edges of the heart are extracted and matched. The result of the matches between pairs of points in the images of the sequence is used to estimate a 4D polar transformation.

2.1. Matching the feature points

The matching method is an enhancement of the iterative closest point (Besl and McKay, 1992; Zhang, 1994; Feldmar and Ayache, 1996), adapted to our problem. Given a point P (x, y, z) in cartesian coordinates and a time value t, the transformation gives a point Q (x', y', z') which is assumed to be the location of point P at time t. To estimate a 4D planispheric transformation f, we therefore need to know the matches between points P_l of the first image ($t=0$) and points $Q_{n,l}$ of the image at time n ($t=t_n$). We thus look for f so that

$$f(P_l,t_n) \simeq Q_{n,l}$$

We define a criterion:

$$C(f)=\sum_{n=0}^{T-1}\sum_{l=0}^{N-1}\alpha_{n,l}\,.\,d[\,f(P_l,t_n)\,;\,\mathrm{CP}_n(f(P_l,t_n))\,]^2. \qquad (11)$$

CP_n calculates the closest point to a 3D point among the feature points FP_n extracted in image n. We use kd-trees to compute this function (Preparata and Shamos, 1985). The criterion is the sum of the residual distances between the estimated location of the points P_l at time t_n and the feature points extracted in Image n. $\alpha_{n,l}$ is a weighting coefficient which depends only on (P_l, t_n) (figure 8). In our experiments, the model is the list of data points at end diastole.

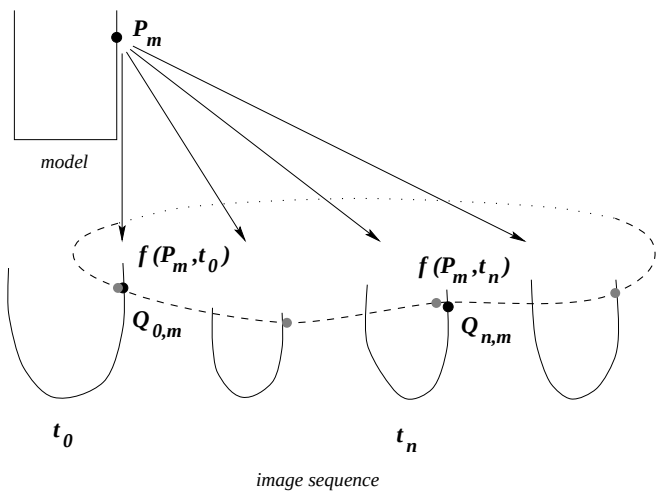

Figure 8. The matching criterion measures the sum of distances between $f(P_l,\ t_n)$, the estimated point P_l at time t_n and $Q_{n,l}$, the closest feature point of Image n, for all existing P_l and t_n.

2.2. Minimizing the criterion

The minimization process is iterative, given an initial transformation f_0. This initial transformation is chosen in our experiments to be the identity (nothing moves anywhere !). Each iteration k splits into three steps:

1. For each 4D point (P_l, t_n), we calculate $f_{k-1}(P_l,t_n)$ (which should be the location of point P_l at time t_n) and we identify its closest feature point $CP_{n,l}$ in Image n. We therefore end up with a list of possible pairs of matched points.

2. For each time t_n and for each type of boundary (endocardium, epicardium), we calculate the residual distance $\| f_{k-1}(P_l, t_n) - CP_{n,l} \|$ for each pair, and we decide whether a pair is reliable or not: we first eliminate pairs for which the residual distance exceeds a fixed threshold. Second, we compute the mean μ and the standard deviation σ attached to the remaining pairs. We then eliminate the points for which the distance is greater than another threshold depending on the distance distribution ($\mu + c.\sigma$, where c can be easily set using a χ^2 table (Feldmar and Ayache, 1996; Feldmar, 1995)).

   We get for this iteration a list S_k of reliable pairs of matched points. Notice that if a point is not matched in this iteration, it may be matched in one that follows.

3. With the filtered list S_k of pairs of points, we calculate f_k which is the best least squares fit for the pairs of points.

The iterative process stops when a maximum number of iterations is reached, or when $S_k = S_{k-1}$. (Feldmar and Ayache, 1996; Feldmar, 1995) gives further details about this adaptation of the iterative closest point algorithm, for instance about the convergence properties.

2.3. Definition of the closest point

The matching function CP_n takes into account for each point its geometric position and the local direction of the intensity gradient calculated while extracting the edges. Considering 2 oriented points $(P;n_P)$ and $(Q;n_Q)$, where n_P and n_Q are the directions of the intensity gradient at point P and Q respectively, the distance between them is calculated as follows:

$$d(P,Q)^2 = \alpha.\|PQ\|^2 + \|n_P - n_Q\|^2 \qquad (12)$$

where α is a weighting coefficient for normalisation. The local direction of the gradient defines which border a points belongs to: if the gradient is oriented towards the center, the point belongs to the endocardium. If not, it is assumed to belong to the epicardium. This separation avoids mismatches between points of two different boundaries and speeds up the computation: one kd-tree is more costly to manipulate than two kd-trees of half size.

This double definition of a point (location + direction) refines the matching criterion and makes it more robust and precise. We know that such features must be used with caution, especially when trying to define a distance between two features (Pennec and Ayache, 1996). However, the formula (12) must be written as a sum of squares in order to keep the convergence properties of the process (Feldmar and Ayache, 1996; Feldmar, 1995).

2.4. Computing an optimal 3D-planispheric coordinate system

A keypoint in the estimation of the 4D transformation is the definition of a 3PC system (a center, a base, an apico-basal vector, a septo-lateral vector and a normalisation factor σ_r).

2.4.1. The coordinate system

In (Declerck *et al.*, 1996), we define a method to align a SPECT heart image with a template using a non-rigid transformation. This method gives a transformation from the normalized coordinates of the template to the patient's case.

As the transformation which deforms the template is sufficiently free (B-spline tensor product), the template can be chosen as a rough approximation of a LV. Here, we choose two truncated ellipsoids (one for the endocardium and one for the epicardium). The parameters have been set manually not to design a precise shape: the idea is just to have a "good-looking" one. We define for this template a center, a basis point and a point in the lateral wall so that all three define a reference system $[C, u, v]$.

The template is matched with the edges of the image of the heart at end diastole (largest volume). With this transformation, we deform the reference system of the template to the patient case (figure 9). Calling S (for "shape") the spline

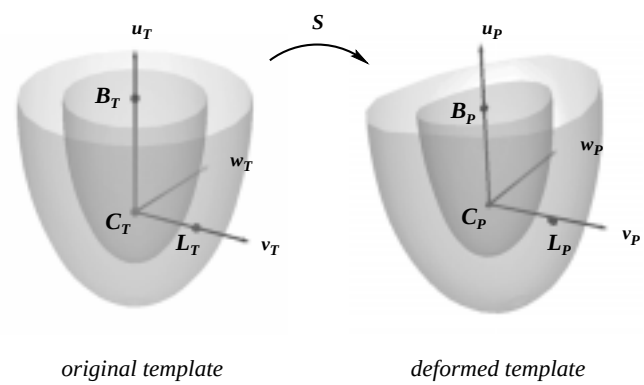

Figure 9. The template and three points defining the coordinate system. By the transformation S, they are deformed to match the shape of the left ventricle of the patient.

transformation deforming the template to the patient's case, the reference system is defined as follows:

- For the template
  - center: C_T
  - base: B_T
  - lateral point : L_T
  - apicobasal vector : $u_T = \dfrac{C_T B_T}{\|C_T B_T\|}$

- – septo-lateral vector : $v_T = \dfrac{C_T L_T}{\|C_T L_T\|}$

  (L_T is such that $u_T . v_T = 0$)
- – infero-anterior vector : $w_T = u_T \times v_T$

- For the patient's case
  - – center : $C_P = S(C_T)$
  - – base : $B_P = S(B_T)$
  - – lateral point : $L_P = S(L_T)$
  - – apicobasal vector : $u_P = \dfrac{C_P B_P}{\|C_P B_P\|}$
  - – septo-lateral vector :

    $$v_P = \frac{C_P L_P - < u_P | C_P L_P > . u_P}{\| \ldots \|}$$

    (so that $u_P . v_P = 0$)
  - – infero-anterior vector : $w_P = u_P \times v_P$

2.4.2. Choosing σ_r

The normalisation factor σ_r is used to make the R coordinate dimensionless, as are the other coordinates X and Y. Changing σ_r changes the shape of a surface in the planispheric geometry by a scaling in the R direction (the lower σ_r, the "higher" the surface). The closest point in this surface to a given point P varies with σ_r (figure 10):

- When σ_r approaches 0, the R value becomes very large compared to X and Y, Q_0, the closest point to P tends to a point with the same R (figure 10, left). This implies that if we use those matches for the least square criterion on distances, the tangential motions (those which change only X and Y) are privileged and the radial motion (those which change only R) becomes negligible.
- When σ_r tends to infinity, the R value becomes very small compared to X and Y. Q_∞, The closest point to P is a point with same X and Y (figure 10, right). This implies that if we use those matches for the least square criterion on distances, the radial motion is privileged and the tangential motions are negligible.

Giving a value to this factor therefore amounts to choosing a weighting between purely tangential and purely radial motions.

As the latitude of the basal points approaches $\pi/2$, the absolute values of X and Y do not exceed 0.5. For an average heart, it appears that the maximum distance (meaning the r value) of a point of the myocardium to the axis does not exceed CB. We thus choose $\sigma_r = 2.CB$, so that R does not exceed 0.5 as for X and Y.

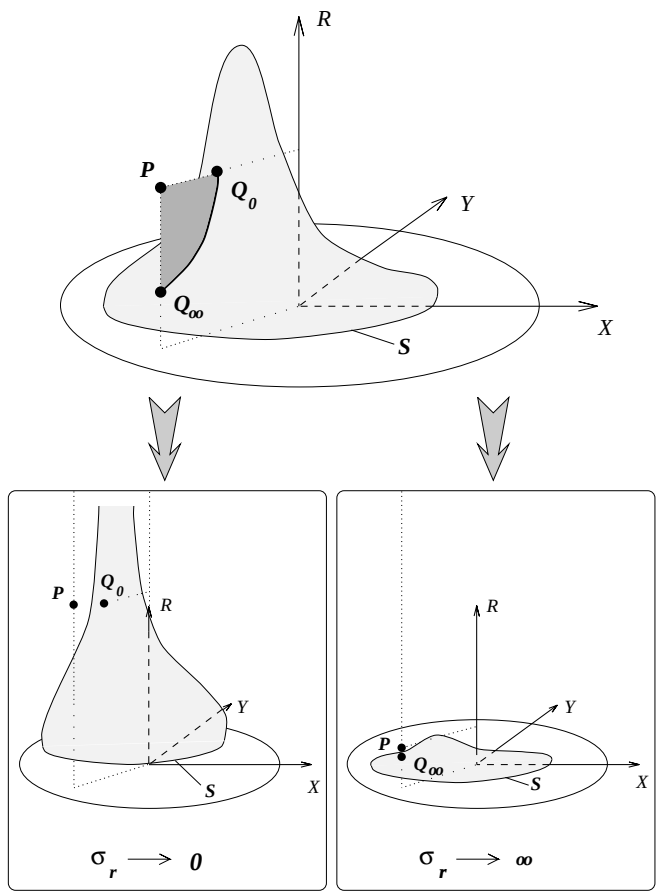

Figure 10. The surface S is represented in 3PC. In this geometry, the location of the closest point Q to P of surface S depends on σ_r. Q belongs to the curved segment $[Q_0 Q_\infty]$, where Q_0 and Q_∞ are the closest point to P for $\sigma_r = 0$ and ∞ respectively. Figure reprinted with kind permission of IEEE *Trans. on Med. Imag.*

3. EXPERIMENTS

We present here experiments conducted on a series of gated SPECT image sequences provided by Pr. M.L. Goris, Stanford University Hospital (California, USA). There are 8 images in the sequence, the size of the images is 64x64x64, pixel size is 2.5mm isotropic. The temporal sampling is uniform and covers the entire cardiac cycle.

3.1. Extraction of feature points

Each image of the sequence is resampled in the polar geometry defined in (Declerck *et al.*, 1996). This reference describes a method to extract edges in nuclear medicine myocardial perfusion images, we recall here the main ideas: in a polar geometry with a center well inside the cavity, the heart looks like a thick plate. We detect edges in this image with a Canny-

Deriche recursive filter (Monga *et al.*, 1991). Cardiac boundary points are easily detected and filtered in this geometry: in an ideal situation, where the heart is a volume of pixels with high intensity values in an image with a high signal-to-noise ratio, starting from the center of the cavity along a radius, the first edge is assumed to belong to the endocardium, the following edge is assumed to belong to the epicardium (figure 11).

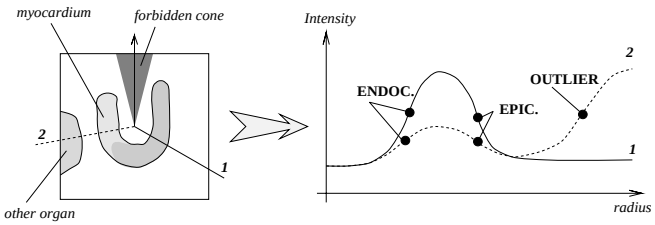

Figure 11. Intensity profiles along 2 different radii starting from the center of the image. The black dots show on both curves the edges detected with the Canny-Deriche filter. On curve 2, the non-cardiac edge is rejected. Figure reprinted with kind permission of IEEE *Trans. on Med. Imag.*

This heuristic constraint is used to filter out the non-cardiac edges (in SPECT images, there may be some parts of the liver, or artificial edges generated by binary masks). In (Declerck *et al.*, 1996), the method is tested on a database of 40 pairs of images, the proportion of erroneous edges was estimated satisfactory enough for the matching process to work. Figure 12 shows the result of the extraction of feature points on four different times of a gated SPECT sequence of a healthy heart.

3.2. Retrieval of trajectories

From these data points, we look for a periodic 4D polar transformation with $n_r = 2$, $n_\theta = 3$, $n_\phi = 6$, $n_t = 5$ (which gives 715 control points, for roughly 50000 data points). Figure 14 shows the surface of a healthy LV (VANN) deformed by the 4D polar transformation. This is the surface of a template matched with the method defined in (Declerck *et al.*, 1996). Because the feature points we extract from the images are not structures, it is difficult to visualise them efficiently. The trajectories of the points are smooth and periodic, as illustrated by figure 13. Figure 15 shows the surface of a pathological LV (BOJO, suffering from septal akinesia due to an infarct) deformed by another 4D transformation: the akinesia is revealed by the relative short trajectories of points around the septum (on the left in each frame of figure 15).

Extracting feature points takes around 20 seconds per image on a DEC Alpha 400 MHz workstation. The computation of the 4D planispheric transformation takes around 15 minutes on the same machine.

3.3. Analysis of the motion

We show in figure 16 a display of the physical parameters values on the surfaces of the heart. On the top, the normal VANN case and on the bottom, the pathological BOJO case. For the radial motion, the values vary between 0 and 40 %, for the elevation, between -5 % and 5 % and for the apico-basal rotation, from -10 to 10 degrees. The values are computed at end systole.

In figure 17, we show a display of the amplitude and the phase of the first harmonic of the radial motion for three normal hearts (CRIR, HUVM and VANN) and a pathological one (BOJO). This crude Fourier analysis shows how the parameter varies over the whole sequence. For the normal cases, there is a variability in the computed values of the parameters:

1. around the base, the values are hasardous due to a bad identification of the base, potentially leading to mismatches. A better segmentation of the base should avoid this kind of behaviour;

2. apart from this region, the distribution of amplitude values is coherent for the three cases, showing that the septum contracts less than the other walls and that the contraction is more important on the endocardium than on the epicardium. The amplitude reveals potential *akinetic* areas;

3. the phase reveals potential *dyskinetic* regions. The values distribution shows the septum contracts slightly later than the other walls. This is particularly visible on cases VANN and HUVM.

However, those values must be interpreted with caution. As the matching procedure works with a closest point method, the tangential motions which are retrieved are not fully reliable (elevation and apico-basal rotation). As a matter of fact, only the radial motion (an "orthogonal" motion) matches what can be expected from a healthy heart (Park *et al.*, 1996; Young *et al.*, 1994) and figure 17 shows, for a pathological case, the sensitivity of this parameter:

- *amplitude*: the septum appears in dark blue, featuring low values. The akinesia is thus located and quantified;
- *phase*: around the septum, the values distribution shows strong variations, due to the fact that the amplitudes are low in this area: the approximation of a nearly flat curve (showing the evolution of the parameter over time) by a sinusoid is therefore very sensitive.

3.4. Perspectives for the validation

The motion we are able to retrieve and analyse using gated-SPECT images sequences must be interpreted with caution.

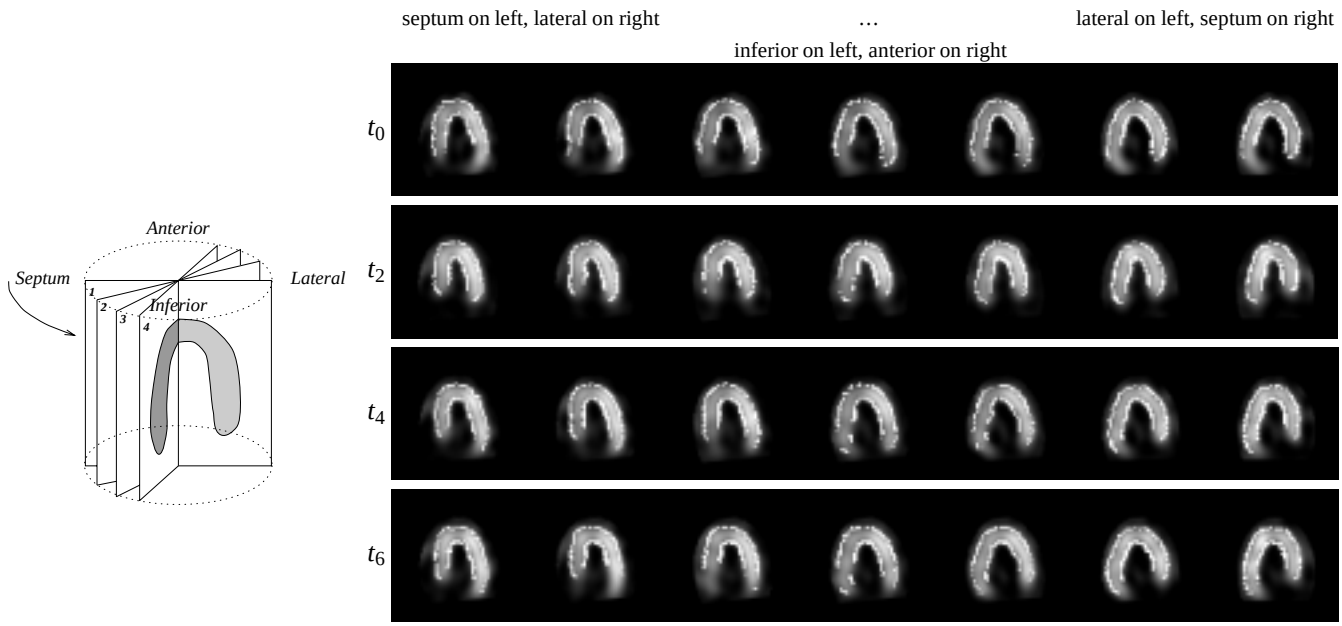

Figure 12. Edges (in white) automatically extracted and filtered from images at four different times (one time per row). On each row, we see central slices resampled from the 3D image by rotation around the apex-base axis, as shown on drawing on the left: this makes easier the display of the myocardial structure.

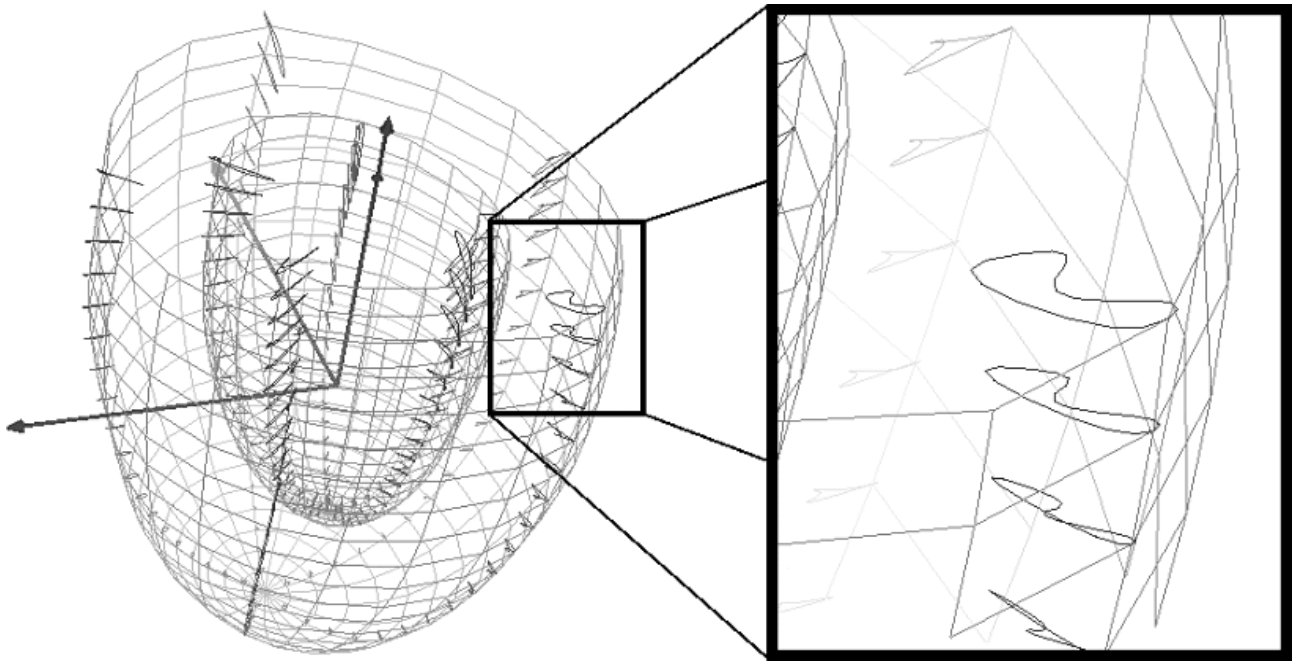

Figure 13. View of the LV from the apex. The trajectories of some points are drawn over the cycle: they are smooth and periodic (see the zoomed area on the right). Figure from (Declerck *et al*,1997).

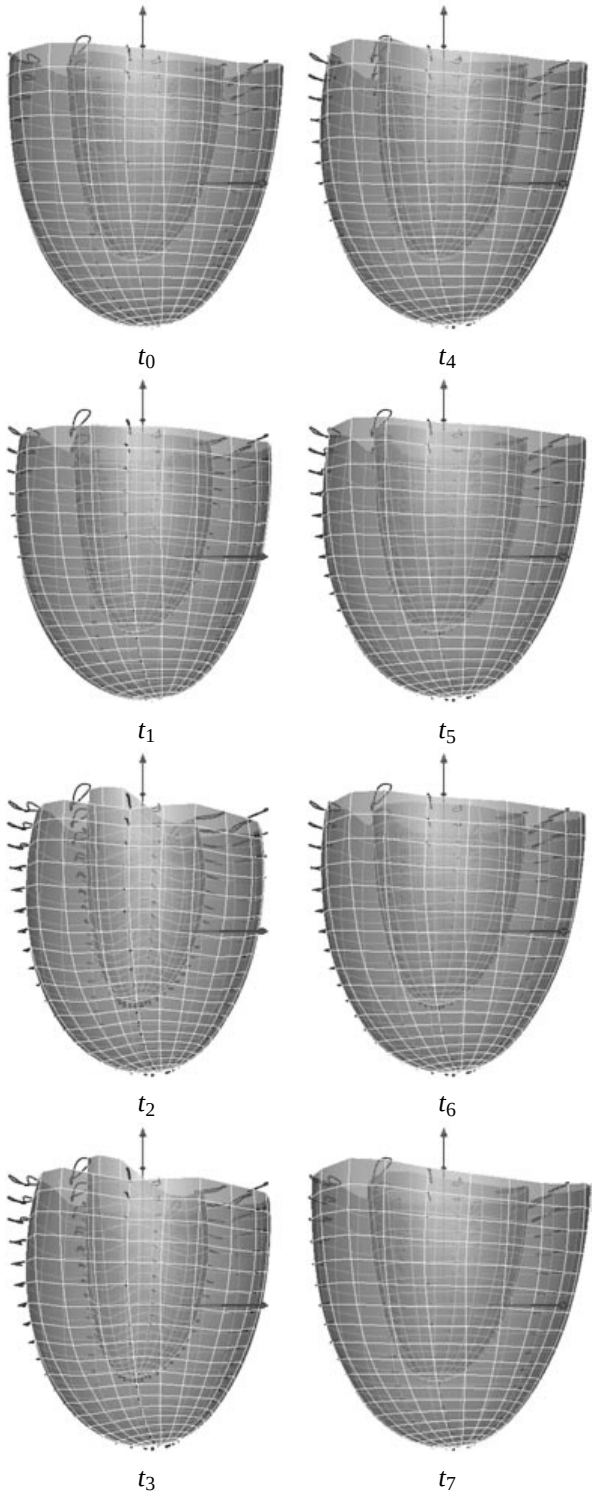

Figure 14. The surface of the LV deformed by the 4D transformation over the 8 times of the sequence. The heart is healthy (**VANN**). Trajectories are represented for some points.

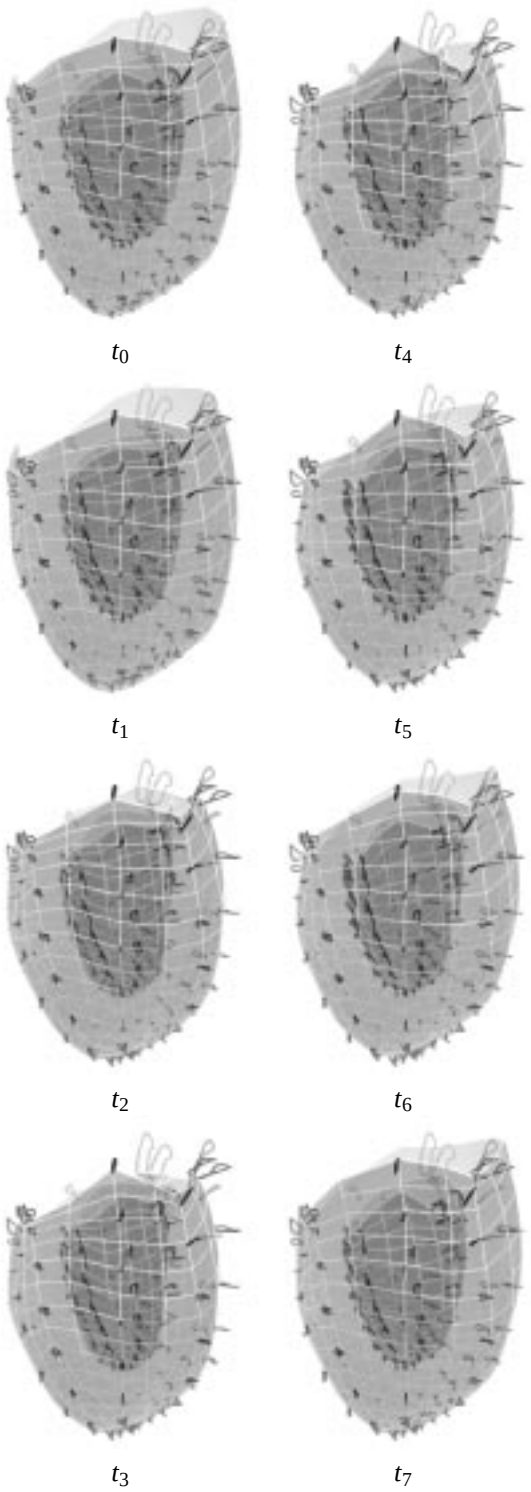

Figure 15. Same as figure 14, for a pathological case (**BOJO**).

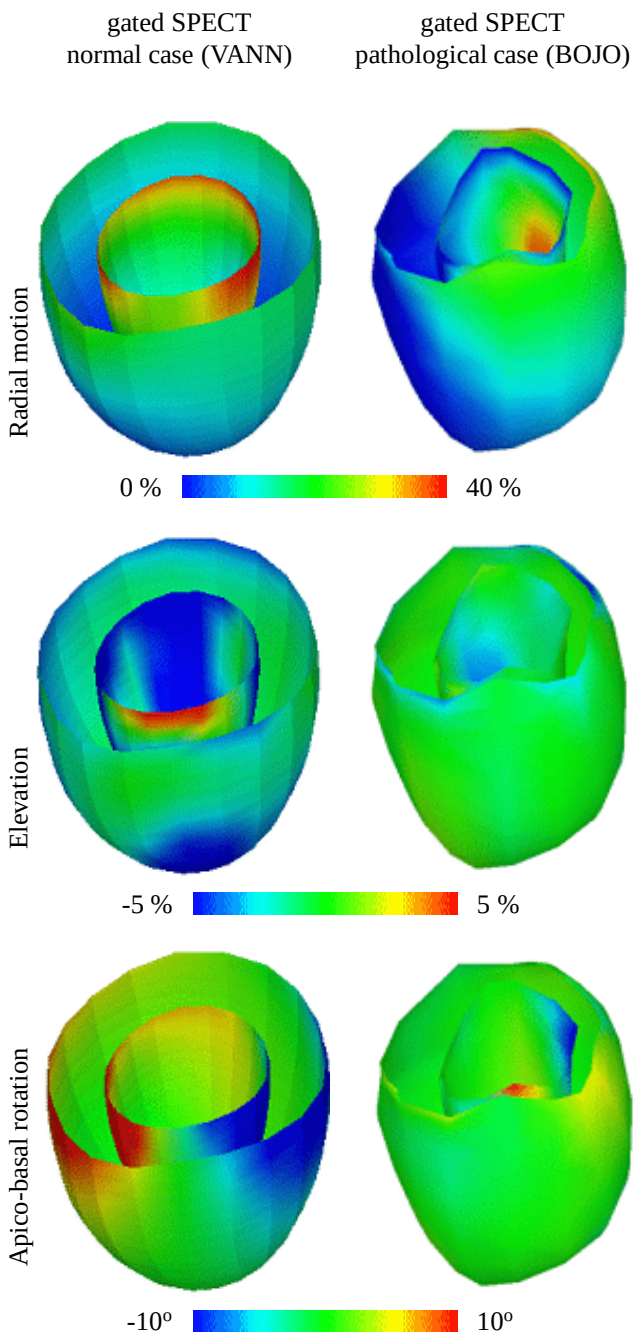

Figure 16. The surface of the heart (the septum is on the left) colorised with the parameters values at end systole, for a normal case (**VANN**, on the left) and for a pathological case (**BOJO**, on the right): **top**, the radial motion, **middle**, the elevation and **bottom**, the apico-basal rotation. The colorscales under the images indicate increasing values from left to right. Figure from (Declerck *et al*,1997).

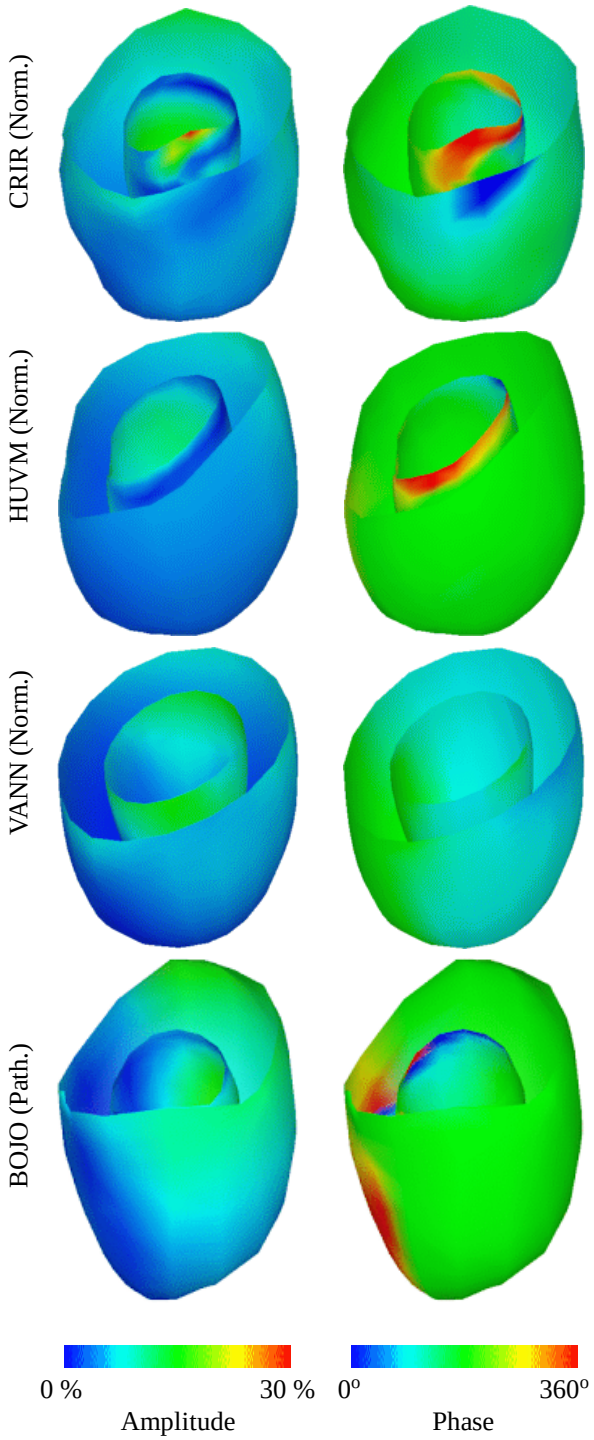

Figure 17. The surface of the heart (the septum is on the left) colorised with the amplitude (**left**) and phase (**right**) of the first harmonic of the radial motion. First 3 lines show normal cases (**CRIR**, **HUVM** et **VANN**), the last line, a pathological one (**BOJO**). The amplitude shows how wide the motion is, the phase shows the synchronisation.

Due to the low resolution of the images, it is difficult to get a precise information. Second, any tangential motion cannot be reliably retrieved using only feature-based techniques without markers. The parameters we are able to compute may be useful if there is a possibility to demonstrate that they can be used for a detection of a pathology, by separating normal and abnormal hearts into two statistically different classes. This validation should be processed on a dataset of heart images of which the pathology or healthy state is known. For a given database, the sensitivity and the specificity can be calculated and can show the usefulness of our approach on a quantitative basis.

Another way to validate our decomposition of the motion is to check that it corresponds to a real motion. Tagged MRI yields images in which the motion of soft tissues at a number of discrete points is easily detectable, can be measured (McVeigh, 1996; Kraitchman *et al.*, 1995; Young *et al.*, 1995; Young *et al.*, 1994; Denney and Prince, 1994) and then compared to our computed motion.

These two validation processes are currently under study, partial results have been obtained (Declerck, 1997) and will be the subject of a forthcoming article.

4. CONCLUSION

In this work, the mathematical framework for a new class of transformation is defined: a 4D planispheric transformation is a differentiable function in space and time coordinates and potentially periodic in time. A small number of parameters constrain the definition of the function and there is a simple relationship between the estimated parameters a_p and the "canonical" motions defined for a moving LV (radial motion, rotation, elevation). We demonstrated the feasability of the method on a series of gated SPECT sequences.

This will be the basis for a number of experimental studies both on nuclear medicine and tagged MR data in collaboration with Pr. Michael Goris (Stanford University Hospital) and Dr. Elliot McVeigh (Johns Hopkins University).

In order to refine the tracking procedure, we are also working on defining feature points **inside** the myocardium. Those points added to the edges we have already defined will give landmarks in the entire myocardial volume and not only on its boundary.

ACKNOWLEDGEMENTS

We want to thank Pr. Michael L. Goris for his precious advices we had and the team of the Stanford University Hospital (California, USA) for providing us with the images.

We give also special thanks to Dr. Eric Bardinet and Pr. Mike Brady for the constructive discussions and comments about the project.

This work was partially supported by regional grant of the Région Provence Alpes Côte d'Azur (doctoral research contract).

A. 3D PLANISPHERIC COORDINATES

This section is dedicated to the problem of finding H_P given a point P in space. In order to avoid cumbersome notation, we rename H_P as H. The problem is, given two points C and B and a point P, to find a point H on the line CB so that:

$$\begin{aligned}(BC, HP) &= \theta \\ CH &= (1-cos\theta).CB\end{aligned}$$

Let us define λ as follows:

$$\overline{CH} = \lambda.\overline{CB} = \lambda.l$$

Because λ is supposed to be equal to $1-cos(\theta)$, $\lambda \in [0,2]$.

If we write

$$CP = \begin{pmatrix} x.l \\ y.l \\ z.l \end{pmatrix} \qquad \text{and} \qquad u = \begin{pmatrix} u_x \\ u_y \\ u_z \end{pmatrix}$$

we have

$$HP = l.\begin{pmatrix} x-\lambda.u_x \\ y-\lambda.u_y \\ z-\lambda.u_z \end{pmatrix}$$

so

$$\begin{aligned}u.HP &= u.HC + u.CP \\ &= l.[-\lambda + (x.u_x + y.u_y + z.u_z)]\end{aligned}$$

On the other hand,

$$cos(\theta) = \frac{BC.HP}{||BC||.||HP||}$$

If we call

$$\begin{aligned}r &= ||HP|| \\ &= l.\sqrt{(x-\lambda.u_x)^2 + (y-\lambda.u_y)^2 + (z-\lambda.u_z)^2}\end{aligned}$$

and

$$p = u.CP$$

we thus have

$$cos(\theta) = -\frac{u.HP}{r}$$

and the constraint (1) can be rewritten, after some calculation,

$$\lambda = \frac{r+p}{r+1} \tag{13}$$

Let us call f a function of λ

$$f(\lambda) = \frac{r(\lambda)+p}{r(\lambda)+1} - \lambda \tag{14}$$

We look for λ_0 so that

$$f(\lambda_0) = 0 \tag{15}$$

To solve this equation, we use a Newton method. In the following lines, we demonstrate that the derivative f' is of a constant sign, which implies a unique solution for (15), if it exists.

The derivative of the function f with respect to λ is as follows

$$f'(\lambda) = \frac{r'(\lambda)(1-p)}{(r(\lambda)+1)^2} - 1$$

It is straightforward to prove that

$$r'(\lambda) = \frac{\lambda - p}{r(\lambda)}$$

so we have

$$f'(\lambda) = \frac{(\lambda-p)(1-p)}{r(\lambda)(r(\lambda)+1)^2} - 1 \tag{16}$$

Let us call P' is the projection of P on (CB). We have then

$$\lambda - p = -\frac{\overline{HP'}}{l}$$

$$1 - p = -\frac{\overline{BP'}}{l}$$

To prove the constant sign of f', we just have to compare the two distance products $CB.\overline{HP'}.\overline{BP'}$ (the numerator of the fraction) and $HP.(HP+CB)^2$ (the denominator of the fraction). If we can prove that $CB.\overline{HP'}.\overline{BP'} < HP.(HP+CB)^2$, the fraction is lower than 1 and f' is negative.

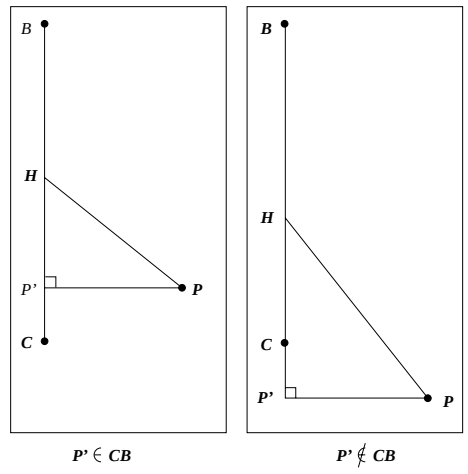

Figure 18. Two possible configurations for P'.

Due to the symmetry of the problem, we can suppose without any loss of generality that P' is on the semi-line $[BC)$. The demonstration of the inequality splits in two parts:

- $P' \in [CB]$ (figure 18, left). We obviously have

$$\begin{array}{rcccl} P'B & < & CB & < & HP+CB \\ CB.P'B & < & CB^2 & < & (HP+CB)^2 \end{array}$$

  as $HP' < HP$,

$$CB.HP'.P'B < HP.(HP+CB)^2$$
$$CB.\overline{HP'}.\overline{BP'} < HP.(HP+CB)^2$$

  this what we want;
- $P' \notin [CB]$ (figure 18, right). We have

$$\begin{array}{rcl} (HP+CB)^2 & > & (HP'+CB)^2 \\ & > & (CP'+CB)^2 = P'B^2 \\ & > & P'B.CB \end{array}$$

  as $HP' < HP$,

$$CB.HP'.P'B < HP.(HP+CB)^2$$
$$CB.\overline{HP'}.\overline{BP'} < HP.(HP+CB)^2$$

  this what we want.

So, in any configuration of P, for any λ, $f'(\lambda) < 0$. f is then a decreasing function.

Obviously,

$$f(0) = \frac{CP + u.CP}{CP + CB} > 0$$

and, if P' is on the semi-line $[BC)$,

$$\begin{aligned} f(1) &= \frac{BP + u.CP}{BP + CB} - 1 \\ &= \frac{u.CP - CB}{BP + CB} \\ &= \frac{u.BP}{BP + CB} < 0 \end{aligned}$$

$f(0)$ and $f(1)$ are of opposite signs, the sign f' is constant, there is then a unique solution for (15).

In our implementation, we use a Newton method to find λ_0 solution of (15). Starting from a central position ($\lambda = 1$), after 3 or 4 iterations, the difference between two successive estimations of λ do not exceed 10^{-6}. The convergence is extremely fast.

B. PROLATE SPHEROIDAL COORDINATES

We define a center O and two "focal points" F_1 and F_2, F_2 being at the same distance δ from O as F_1, but in the opposite direction. A prolate sphere is defined to have a constant radius λ (dimensionless number), a point in this prolate sphere is defined fixing two angles: elevation θ and azimuth ϕ. From these three parameters, the cartesian coordinates (x, y, z) of this pont are calculated using the following formulae:

$$\begin{aligned} x &= \delta \sinh(\lambda) \sin(\theta) \cos(\phi) \\ y &= \delta \sinh(\lambda) \sin(\theta) \sin(\phi) \\ z &= \delta \cosh(\lambda) \cos(\theta) \end{aligned} \tag{17}$$

Conversely, knowing the cartesian coordinates (x, y, z), it is possible to compute the prolate spheroidal parameters (λ,θ,ϕ) using the equations:

$$\begin{aligned} r_1 &= \sqrt{x^2 + y^2 + (z - \delta)^2} \\ r_2 &= \sqrt{x^2 + y^2 + (z + \delta)^2} \\ \lambda &= \operatorname{acosh}\left(\frac{r_1 + r_2}{2.\delta}\right) \\ \theta &= \operatorname{acos}\left(\frac{r_1 - r_2}{2.\delta}\right) \\ \phi &= \operatorname{atan2}\left(\frac{x}{\delta \sinh(\lambda) \sin(\theta)}, \frac{y}{\delta \sinh(\lambda) \sin(\theta)}\right) \end{aligned} \tag{18}$$

Analogously to our system, F_1 would be C, O would be B, F_2 would be C' (figure 7) and λ would be R. In the end, the transformation from (R,θ,ϕ) coordinates to (X,Y,R) would be expressed as in (2).

REFERENCES

Amini, A. and Duncan, J. (1992). Bending and stretching models for LV wall motion analysis from curves and surfaces. In *Image and Vision Computing*, Vol. 10, pp. 418–430.

Arts, T., Hunter, W.C., Douglas, A., Muijtjens, A.M., and Reneman, R.S. (1992). Description of the deformation of the left ventricle by a kinematic model. *Journal of Biomechanics*, 25(10), 1119–1127.

Bardinet, E., Cohen, L.D., and Ayache, N. (1995). Tracking medical 3D data with a parametric deformable model. In *IEEE Computer Vision Symposium*.

Bardinet, E., Cohen, L.D., and Ayache, N. (1996). Tracking and motion analysis of the left ventricle with deformable superquadrics. *Medical Image Analysis*, 1(2), 129–149. (also INRIA research report #2797).

Benayoun, S., Nastar, C., and Ayache, N. (1995). Dense non-rigid motion estimation in sequences of 3D images using differential constraints. In *Computer Vision, Virtual Reality and Robotics in Medicine*, Vol. 905 of *Lecture Notes in Computer Science*, pp. 309–318. Springer-Verlag.

Besl, P. and McKay, N. (1992). A method for registration of 3D shapes. *IEEE Transactions on Pattern Analysis and Machine Intelligence*, 14, 239–256.

Clarysse, P., Jaouen, O., Magnin, I., and Morvan, J.M. (1995). 3D Boundary Extraction of the Left Ventricle by a Deformable Model with a priori Information. In *IEEE International Conference on Image Processing*.

de Murcia, J. (1996). *Reconstruction d'images cardiaques en tomographie d'émission monophotonique à l'aide de modèles spatio-temporels*. *Ph.D. Thesis*, Institut National Polytechnique de Grenoble.

Declerck, J. (1997). *Étude de la dynamique cardiaque par analyse d'images tridimensionnelles*. *Ph.D. Thesis*, Université Nice-Sophia Antipolis.

Declerck, J., Feldmar, and Ayache, N. (1997). Definition of a 4D continuous polar transformation for the tracking and the analysis of LV motion. In *Computer Vision, Virtual Reality and Robotics in Medicine II - Medical Robotics and Computer Assisted Surgery III*, Vol. 1205 of *Lecture Notes in Computer Science*, pp. 33–42. Springer-Verlag.

Declerck, J., Feldmar, J., Goris, M.L., and Betting, F. (1996). Automatic registration and alignment on a template of cardiac stress

& rest SPECT images. In *Mathematical Methods in Biomedical Image Analysis*, pp. 212–221. (Also INRIA Research Report # 2770. Accepted for publication in IEEE Transactions on Medical Imaging).

Denney, T.S. and Prince, J.L. (1994). 3D displacement field reconstruction from planar tagged cardiac MR images. In *IEEE Workshop on Biomedical Image Analysis*, pp. 51–60.

Farin, G. (1989). *Curves and Surfaces for Computer Aided Geometric Design*. Academic Press, Inc.

Feldmar, J. (1995). *Recalage rigide, non-rigide et projectif d'images médicales tridimensionnelles*. *Ph.D. Thesis*, Ecole Polytechnique.

Feldmar, J. and Ayache, N. (1996). Rigid, affine and locally affine registration of free-form surfaces. *Computer Vision and Image Understanding*, 18(2), 99–119. (Also INRIA Research Report # 2220).

Goldgof, D., Lee, H., and Huang, T. (1988). Motion analysis of nonrigid surfaces. In *IEEE Computer Vision and Pattern Recognition*, pp. 375–380.

Gorce, J.M., Friboulet, D., and Magnin, I.E. (1997). Estimation of three-dimensional cardiac velocity fields: assessment of a differential method and application to 3-D CT data. *Medical Image Analysis*, 1(3), 1–16.

Hunter, P.J. and Smaill, B.H. (1988). The analysis of cardiac function: a continuum approach. *Prog. Biophys. Molec. Biol.*, 52, 101–164.

Kraitchman, D., Young, A., Chang, C.N., and Axel, L. (1995). Semi-automatic tracking of myocardial motion in MR tagged images. *IEEE Transactions on Medical Imaging*, 14(3), 422–433.

Matheny, A. and Goldgof, D. (1995). The use of three- and four-dimensional surface harmonics for rigid and nonrigid shape recovery and representation. *IEEE Transactions on Pattern Analysis and Machine Intelligence*, 17(10), 967–978.

McEachen, J.C., Nehorai, A., and Duncan, J.S. (1994). A recursive filter for temporal analysis of cardiac motion. In *IEEE Workshop on Biomedical Image Analysis*, pp. 124–133.

McInerney, T. and Terzopoulos, D. (1995). A dynamic finite element surface model for segmentation and tracking in multidimensional medical images with application to cardiac 4D image analysis. *Computerized Medical Imaging and Graphics*, 19(1), 69–83.

McVeigh, E. (1996). MRI of myocardial function: motion tracking techniques. *Magnetic Resonance Imaging*, 14(2), 137–150.

Meyer, F.G., Todd Constable, R., Sinusas, A., and Duncan, J. (1995). Tracking myocardial deformation using spatially-constrained velocities. In et al., Y. Bizais (ed.), *Information Processing in Medical Imaging*, pp. 177–188.

Monga, O., Deriche, R., and Rocchisani, J.M. (1991). 3D edge detection using recursive filtering: application to scanner images. *Computer Vision, Graphics and Image Processing*, 53(1), 76–87.

Nastar, C. (1994). Vibration modes for non-rigid motion analysis in 3D images. In *European Conference in Computer Vision*, number 800 in Lecture Notes in Computer Science, pp. 231–236. Springer-Verlag.

O'Donnell, T., Gupta, A., and Boult, T. (1994). A periodic generalized cylinder model with local deformations for tracking closed contours exhibiting repeating motion. In *IEEE Workshop on Biomedical Image Analysis*, pp. 397–402.

Park, J., Metaxas, D., and Axel, L. (1996). Analysis of left ventricular motion based on volumetric deformable models and MRI-SPAMM. *Medical Image Analysis*, 1(1), 53–71.

Park, J., Metaxas, D., and Young, A. (1994). Deformable models with parameter functions: application to heart-wall modeling. In *IEEE Computer Vision and Pattern Recognition*, pp. 437–442.

Pennec, X. and Ayache, N. (1996). Randomness and Geometric Features in Computer Vision. In *IEEE Conf. on Computer Vision and Pattern Recognition (CVPR'96)*, San Francisco, Cal.

Preparata, F.P. and Shamos, M.I. (1985). *Computational geometry, an introduction*. Springer Verlag.

Radeva, P., Amini, A., Huang, J., and Marti, E. (1996). Deformable B-Solids and Implicit Snakes for Localization and Tracking of MRI-SPAMM Data. In *Mathematical Methods in Biomedical Image Analysis*, pp. 192–201.

Risler, J.-J. (1991). *Méthodes mathématiques pour la CAO*. Masson.

Schudy, R. and Ballard, D. (1979). A computer model for extracting moving heart surfaces from four-dimensional cardiac ultrasound images. In *Third International Conference on Computer Vision*, pp. 366–376.

Shi, P., Amini, A., Robinson, G., Sinusas, A., Constable, C.T., and Duncan, J. (1994). Shape-based 4D left ventricular myocardial function analysis. In *IEEE Workshop on Biomedical Image Analysis*, pp. 88–97.

Shi, P., Robinson, G., Chakraborty, A., Staib, L., Constable, R., Sinusas, A., and Duncan, J. (1995). A unified framework to assess myocardial function from 4D images. In *Computer Vision, Virtual Reality and Robotics in Medicine*, Vol. 905 of *Lecture Notes in Computer Science*, pp. 327–337. Springer-Verlag.

Song, S.M., Leahy, R.M., Boyd, D.P., Brundage, B.H., and Napel, S. (1994). Determining Cardiac Velocity Fields and Intraventricular Pressure Distribution from a Sequence of Ultrafast CT Cardiac Images. In *IEEE Transaction on Medical Imaging*, Vol. 13, pp. 386–397.

Thirion, J.-P. (1995). Fast non-rigid matching of 3D medical images. In *Medical Robotics and Computer Aided Surgery*, pp. 47–54.

Todd Constable, R.T., Rath, K.M., Sinusas, A.J., and Gore, J.C. (1994). Development and evaluation of tracking algorithms for cardiac wall motion analysis using phase velocity MR imaging. In *Magnetic Resonance Medicine*, Vol. 32, pp. 33–42.

Waks, E., Prince, J., and Douglas, A. (1996). Cardiac motion simulator for tagged MRI. In *Mathematical Methods in Biomedical Image Analysis*, pp. 182–191.

Young, A., Kraitchman, D., Dougherty, L., and Axel, L. (1995). Tracking and Finite Element Analysis of Stripe Deformation in Magnetic Resonance Tagging. *IEEE Transactions on Medical Imaging*, 14(3), 413–421.

Young, A.A., Kramer, C.K., Ferrari, V.A., Axel, L., and Reichek, N. (1994). Three-dimensional left ventricular deformation in hypertrophic cardiomyopathy. *Circulation*, 90, 854–867.

Zhang, Z. (1994). Iterative point matching for registration of free-form curves and surfaces. *International Journal of Computer Vision*, 13(2), 119–152. Also INRIA Research Report #1658.